REPORT DOCUMENTATION PAGE

The public reporting burden for this collection of information is estimated to average 1 hour per response, including the time for reviewing instructions, searching existing data sources, gathering and maintaining the data needed, and completing and reviewing the collection of information. Send comments regarding this burden estimate or any other aspect of this collection of information, including suggestions for reducing the burden, to the Department of Defense, Executive Service Directorate (0704-0188). Respondents should be aware that notwithstanding any other provision of law, no person shall be subject to any penalty for failing to comply with a collection of information if it does not display a currently valid OMB control number.

PLEASE DO NOT RETURN YOUR FORM TO THE ABOVE ORGANIZATION.

1. REPORT DATE (DD-MM-YYYY)	2. REPORT TYPE	3. DATES COVERED (From - To)
05-11-2012	FINAL	22 Aug 11 – 22 Aug 12

4. TITLE AND SUBTITLE

Fabrication of Cu2O/TiO2 nanotubes heterojunction arrays and investigation of their photoelectrochemical behaviour

5a. CONTRACT NUMBER

W911NF-11-1-0386

5b. GRANT NUMBER

R&D 1506-AM-01

5c. PROGRAM ELEMENT NUMBER

5. AUTHOR(S)

Prof. F. Di Quarto
Prof. M. Santamaria

5d. PROJECT NUMBER

5e. TASK NUMBER

5f. WORK UNIT NUMBER

6. PERFORMING ORGANIZATION NAME(S) AND ADDRESS(ES)

Università degli Studi di Palermo
Dipartimento di Ingegneria Civile, Ambientale, Aerospaziale e dei Materiali
Electrochemical Material Science Laboratory, c/o DICAA
Viale delle Scienze
90128 Palerm, Italy

8. PERFORMING ORGANIZATION REPORT NUMBER

9. SPONSORING/MONITORING AGENCY NAME(S) AND ADDRESS(ES)

USAITC-A
Building 188
86 Blenheim Crescent, Ruislip,
Middlesex, HA4 7HL
UK

10. SPONSOR/MONITOR'S ACRONYM(S)

11. SPONSOR/MONITOR'S REPORT NUMBER(S)

12. DISTRIBUTION/AVAILABILITY STATEMENT

Approved for Public Release, distribution is umlimited

13. SUPPLEMENTARY NOTES

14. ABSTRACT

In the frame of the grant W911NF-11-1-0386, this 4th interim report is focused on the fabrication ofCu2O/TiO2 nanotubes heterojunction arrays to be used in photovoltaic or photoelectrochemical solar cells. The presence of Cu2O nanoparticles on the TiO2 NTs surface may overcome the low charge separation efficiency because of the superior host structure provided spatially by the TiO2 nanotubes array besides their matched energy bands. Moreover, the highly ordered nanotube arrays creates a better opportunity to improve photogenerated carrier lifetime. Thus, starting from previous experimental results on TiO2 nanotubes (see reports prepared for grants noW911NF-09-10461 and W911NF-10-1-0465), we want to develop a procedure able to allow the fabrication of heterojunctions with improved photoelectrochemical properties with respect to those shown by the not functionalized NTs.

15. SUBJECT TERMS

16. SECURITY CLASSIFICATION OF:			17. LIMITATION OF ABSTRACT	18. NUMBER OF PAGES	19a. NAME OF RESPONSIBLE PERSON
a.REPORT	b. ABSTRACT	c. THIS PAGE			
Unclassified	Unclassified	Unclassified		23	**19b. TELEPHONE NUMBER** (Include area code)

Università degli Studi di Palermo

Dipartimento di Ingegneria Civile, Ambientale, Aerospaziale e dei Materiali
Electrochemical Material Science Laboratory

USAITC-A grant W911NF-11-1-0386

4th Interim Report

Fabrication of Cu_2O/TiO_2 nanotubes heterojunction arrays and investigation of their photoelectrochemical behaviour

Prepared by:

Prof. Francesco Di Quarto

Prof. Monica Santamaria

Prepared for:

US ARMY RDECOM ACQ CTR - W911NF

4300 S. MIAMI BLVD

DURHAM NC

Introduction

Titanium dioxide (TiO_2), as an environmentally benign photocatalyst with low cost, has received much attention during the past two decades (1-2). However, TiO_2 suffers from dissatisfactory quantum efficiency. The rapid recombination of photoinduced electron-hole pairs greatly limits the energy conversion efficiency (3). In addition, the wide band gap (3.2 eV for anatase) corresponds to the utilization of only about 5% of sunlight. Therefore, it is very necessary to develop effective solutions to improve the charge separation efficiency and visible-light photoactivity. The idea of forming a heterojunction structure between TiO_2 and a narrow band gap semiconductor with matched band potentials may provide an effective way to address the two issues (4-5). The well-established heterojunction structure could be employed to increase the lifetime of the charge carriers and enhance the quantum yield (6). Meanwhile, the electrons excited by visible light can be transferred to TiO_2 from the narrow band gap semiconductor, which favours the charge separation and also improves the visible-light photocatalytic activity of the heterostructure dramatically. Cuprous Oxide (Cu_2O), a p-type semiconductor, is a promising material for solar energy conversion, micro/nanoelectronics and magnetic storage devices (7-8). Bessekhouad et al. (9) showed that high efficiency of coupled Cu_2O/TiO_2 heterojunction for the photodecomposition of Orange II can be reached. Siripala et al. (10) prepared Cu_2O/TiO_2 heterojunction as a potential thin film photocathode with high activity for hydrogen production. Detailed mechanism of interparticle electron transfer, in Cu_yO_z/TiO_2 heterojunctions, was discussed by Helaïli et al. (11). However, the energy conversion efficiency is relatively low and it is troublesome to separate and recycle the composite powder from the reaction system.

In the frame of the grant W911NF-11-1-0386, this 4th interim report is focused on the fabrication of Cu_2O/TiO_2 nanotubes heterojunction arrays to be used in photovoltaic or photoelectrochemical solar cells. The presence of Cu_2O nanoparticles on the TiO_2 NTs surface may overcome the low charge separation efficiency because of the superior host structure provided spatially by the TiO_2 nanotubes array besides their matched energy bands. Moreover, the highly ordered nanotube arrays creates a better opportunity to improve photogenerated carrier lifetime. Thus, starting from previous experimental results on TiO_2 nanotubes (see reports prepared for grants noW911NF-09-10461 and W911NF-10-1-0465), we want to develop a procedure able to allow the fabrication of heterojunctions with improved photoelectrochemical properties with respect to those shown by the not functionalized NTs.

Experimental

To prepare TiO_2 NTs, titanium sheets (commercially pure, ASTM grade 2) with 0.5 mm thickness were used. Before anodizing, titanium sheets were mechanically polished and etched in a mixture of hydrofluoric acid, nitric acid and water (1:1:3 Vol.) and ultrasonically cleaned in acetone and ethanol and finally, rinsed with deionized water and dried in air. Nanotubes were formed in an ethylene glycol (99.8% anhydrous, Aldrich) solution with addition of 0.25 wt% NH_4F and 0.75 wt% deionized water. Anodizing was conducted in a two-electrode configuration using a platinum mesh as cathode and potential was kept constant during anodizing at 45 V for 10 minutes.

In order to induce crystallization in the prepared nanotubes, a thermal treatment was performed soon after the anodizing process. The layers were heated to 450°C under air exposure, kept for 20 minutes at high temperature and left cooling in the furnace.

Field-Emission Scanning Electron Microscope (FE-SEM) was used to examine the morphology and geometry of nanotube arrays. X-Ray Diffraction technique (XRD) was used to investigate phase transformations in TiO_2 NTs after annealing and as a consequence of the functionalization.

Electrodeposition was performed in a conventional three electrodes cell. The Ti/TiO_2 NTs layer was used as working, while a Pt wire and a silver/silver chloride (E = 0.198 V/SHE) were used as counter and reference electrodes, respectively. The electrochemical deposition was performed in 0.4 M $CuSO_4$ – 3 M lactic acid aqueous solution. The pH was adjusted to 10 adding small amount of 5 M NaOH. The deposition temperature was kept constant at 35°C.

The experimental set-up employed for the photo-electrochemical investigations is described elsewhere (12). It consists of a 450 W UV-Vis Xenon lamp coupled with a motorized monochromator (Kratos), which allows monochromatic irradiation of the specimen surface through the electrochemical cell quartz windows. A two-phase lock-in amplifier (EG&G) was used in connection with a mechanical light chopper (frequency: 13 Hz) in order to separate the photocurrent from the total current circulating in the cell.

Electrochemical impedance measurements were recorded in 0.1 M Na_2SO_4 with $v_{a.c.} = 10$ mV and frequency ranging between 0.1 Hz and 100 kHz.

Results

TiO_2 layers fabrication

As detailed described in previous reports (grants W911NF-09-10461 and W911NF-10-1-0465), titanium oxide nanotubes can be easily grown on etched Ti surface, by anodizing the metal in a

3

fluoride containing electrolyte. We selected to prepare the TiO_2 NTs layers by anodizing chemically etched titanium foils at 45 V for 10 minutes in an ethylene glycol solution. These experimental conditions were found to allow the formation of large arrays of nanotubes with good adhesion to the metallic substrate after thermal treatment. Longer nanotubes (i.e. longer anodizing time) easily detach from the metal substrate during the drying process. As presented in Fig. 1, nanotubes are well ordered and have smooth wall surfaces which are characteristics of nanotubes formed in organic solutions. Because of short anodizing time and fast formation rate of nanotubes, their geometry is not completely ordered and some nanotubes are splitting or merging to form a more uniform structure as usually seen after longer anodizing times.

Figure 1 - Scanning electron microscope image of nanotubes anodized at 45 V for 10 minutes.

As prepared nanotubes show very poor photoelectrochemical activity, thus they were annealed at 450°C for 20 minutes. Soon after annealing, photocurrent spectra were recorded in 0.1 M Na_2SO_4 under chopped light (chopping frequency 13 Hz) at constant polarizing voltage ($U_E = 0.15$ V), as shown in Fig. 2. From the photocurrent spectra it was possible to estimate the band gap values of the TiO2 NTs, by assuming non-direct optical transitions, according to the following eq.:

$$(I_{ph}h\nu)^{0.5} \propto (h\nu - E_g) \tag{1}$$

4

where I_{ph} is the photocurrent yield, proportional to the light absorption coefficient, $h\nu$ is the photon energy. The estimated band gap value (E_g = 3.18 eV) is very close to that reported for anatase (i.e. 3.2 eV).
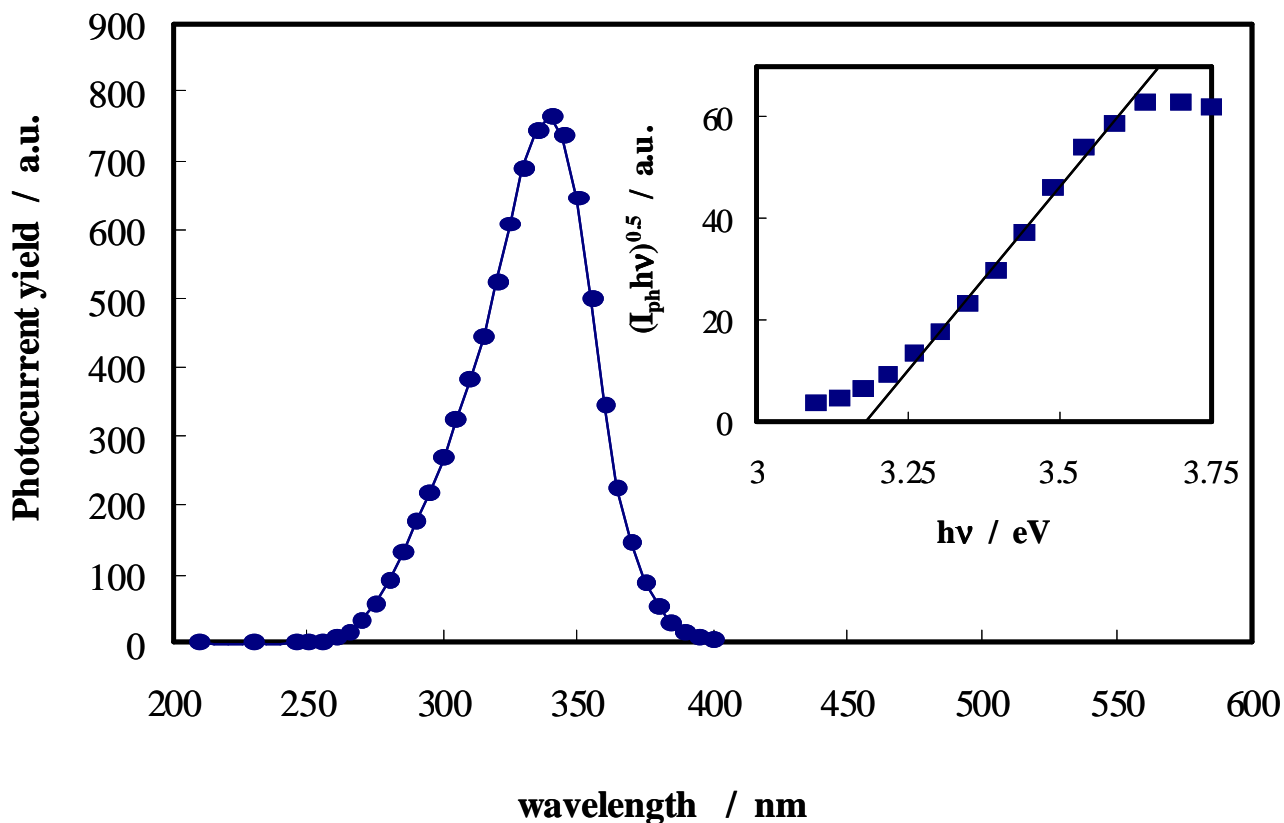

Figure 2 –Photocurrent spectrum relating to TiO_2 nanotubes grown at 45 V for 10 minutes after thermal treatment (20 min 450°C). U_E = 0.15 V in 0.1 M Na_2SO_4. Inset: band gap estimate under the hypothesis of non direct optical transitions.

In Fig. 3a we report the measured photocurrent as a function of time under stationary irradiation recorded by polarizing the Ti/TiO_2 NTs electrodes at 0.15 V in 0.1 M Na_2SO_4. For $\lambda \geq 400$ nm a UV filter was used to avoid a spurious signal due to wavelength doubling. The measured photocurrent diminishes soon after irradiation, thus suggesting the presence of recombination phenomena. To further improve the photocurrent generation efficiency, we tried to reduce the probability of electrons and holes recombination making more efficient the uptaking of photogenerated holes by electrolyte species. Thus, we have introduced in the electrochemical bath employed for the photoelectrochemical experiments some methanol.
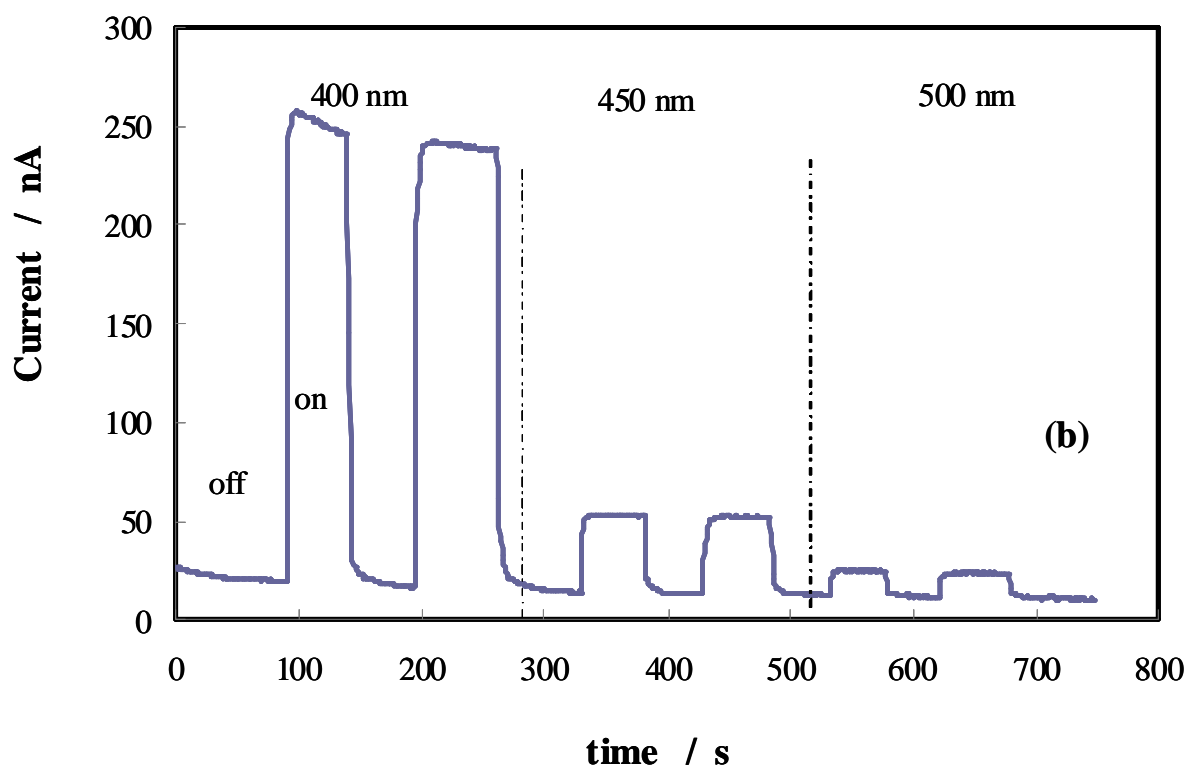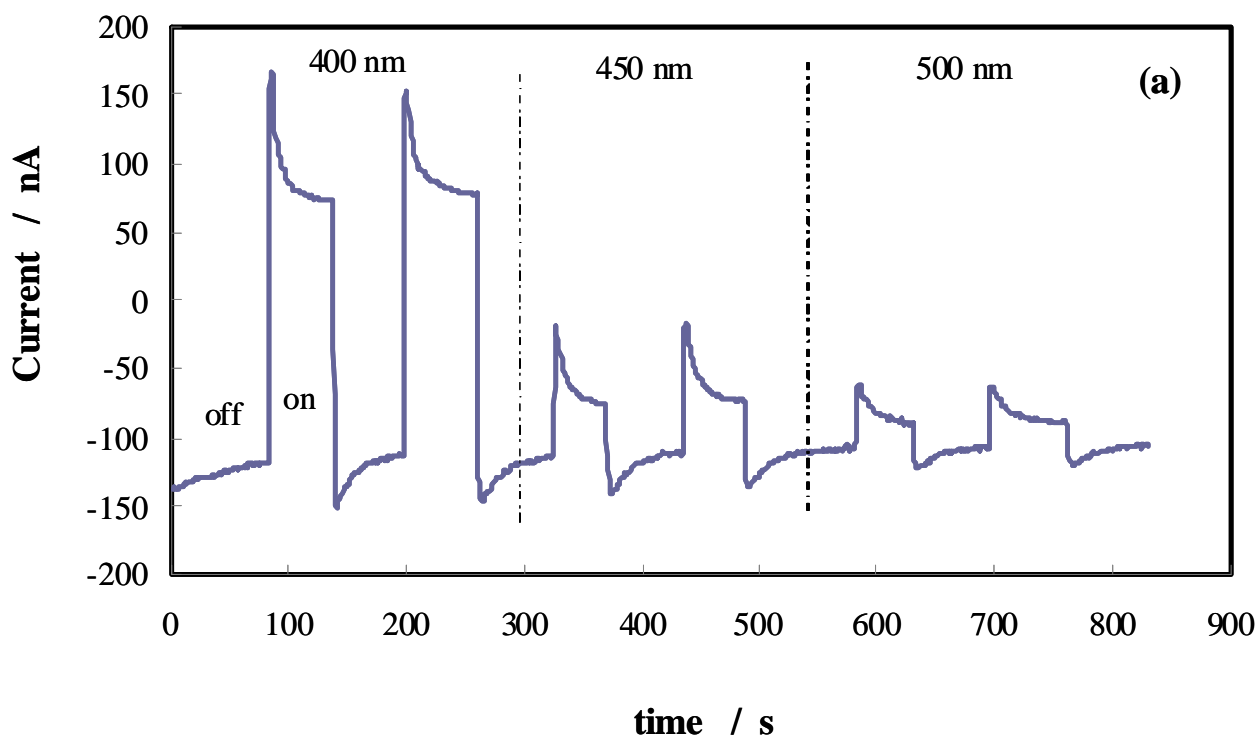
Figure 3 - Current vs time curves relating TiO_2 NTs layer of Fig. 2 recorded at $U_E = 0.15$ V under dark (off) or light (on) irradiation in 0.1 M Na_2SO_4. a) without and b) with the addition of methanol.

As shown in Fig. 3b, the presence of CH_3OH cancel the transient decay of I_{ph} soon after irradiation, even if stationary I_{ph} values are almost coincident with those measured in methanol free solution. In Fig. 4 we report the impedance spectrum in the Bode representation relating to annealed TiO_2 NTs, recorded by polarizing the NTs layer at 0.15 V in 0.1 M Na_2SO_4. We have overlapped to the experimental points the simulated curves according to the equivalent circuit reported in Fig. 5, where R_{el} is the electrolyte resistance, R_{ct} the charge transfer resistance, C_H is the Helmholtz double layer capacitance, R_{ox} the barrier oxide resistance and Q_{ox} accounts for the oxide capacitance.

Figure 4 - Measured and simulated impedance and phase angles values relating to the TiO_2 NTs after thermal treatment, recorded by polarizing the electrode at 0.15 V in 0.1 M Na_2SO_4.
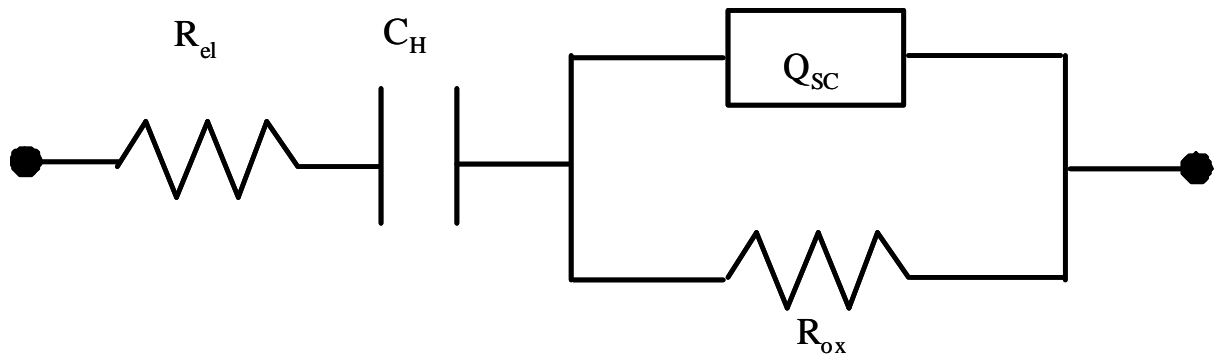

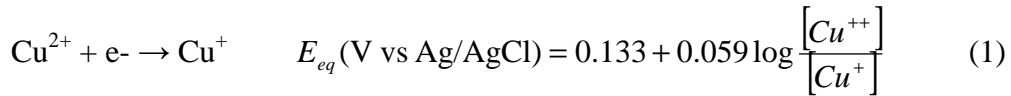**Figure 5** – Equivalent circuit employed to simulate the impedance spectra.

7

Table 1 - Fitting parameters of Fig. 4.

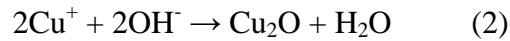| R_{el}	C_H	R_{ox}	Q_{ox}	n
$\Omega\ cm^2$	$\mu F\ cm^{-2}$	$\Omega\ cm^2$	$S\ cm^{-2}$	
143	18.5	$6.0 \cdot 10^4$	$4.76 \cdot 10^{-5}$	0.92

There is a very good agreement between the experimental and the simulated results with the fitting parameters of table 1.

Cu₂O potentiostatic deposition

Cu$_2$O electrodeposition was performed by polarizing the Ti/TiO$_2$ NTs electrodes at U_E = - 0.4 V in the CuSO$_4$ containing bath described in the experimental section. According to the Pourbaix diagram relating to Cu-H$_2$O, at this potential the measured cathodic current can be sustained by the following reduction process:

$$Cu^{2+} + e- \rightarrow Cu^+ \qquad E_{eq}(\text{V vs Ag/AgCl}) = 0.133 + 0.059\log\frac{\left[Cu^{++}\right]}{\left[Cu^+\right]} \qquad (1)$$

with subsequent oxide precipitation according to the following reaction:

$$2Cu^+ + 2OH^- \rightarrow Cu_2O + H_2O \qquad (2)$$

This last step is possible due to the high pH (i.e. high OH$^-$ concentration) of the solution, obtained by the addition of NaOH to electrolyte. The reaction of sodium hydroxide with lactic acid causes the formation of lactate ions, that are reported to form complexes with Cu^{++}, thus keeping very low the concentration of free cupric ions in the electrolyte and hindering the precipitation of Cu(OH)$_2$, which is expected to occur in a so concentrated alkaline CuSO$_4$ solution. If we assume that [Cu^{++}] = [Cu$^+$] = 10^{-6} M, E$_{eq}$ = 0.133 V, which is more anodic with respect to the potential applied during the potentiostatic polarization. Moreover, the very low concentration of free Cu^{++} ions brings the equilibrium potential of Cu/Cu^{++} to - 0.04 V, thus reduction of Cu^{++} to Cu$^+$ is thermodynamically favoured.
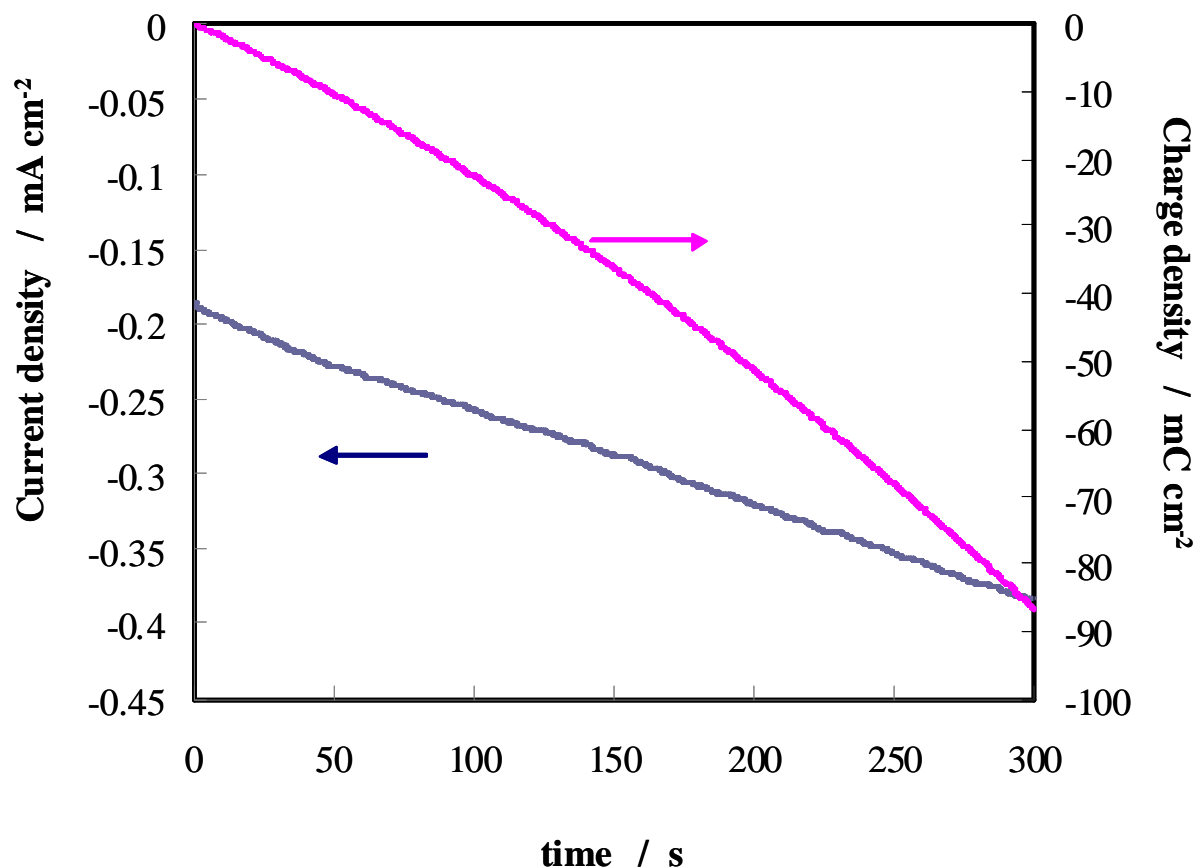
8

Figure 6 – Current density and charge density vs time curves recorded under potentiostatic polarization ($U_E = -0.4$ V) in the electrodeposition solution (see experimental section).

As shown in Fig. 6, in spite of the constant polarizing voltage (i.e. overpotential) the current density increases with increasing time at least up to 5 minutes. This linear dependence suggests that Cu_2O deposition occurs with a very fast nucleation process (instantaneous nucleation, all the electrode sites are converted to nuclei), followed by the growth of the independent nuclei. If these latter are modelled as 2D cylindrical structures (2D nucleus growing only laterally), a current density linearly changing with time is foreseen. The current becomes constant presumably after the whole surface is covered by Cu_2O and the deposited film starts to thicken. This hypothesis is supported by the analysis of the morphological features of the TiO_2/Cu_2O electrodes soon after deposition. At the early stages of the polarization, the TiO_2 nanotubes' surface is covered by nanoparticles, as shown in Fig. 7 for a TiO_2 NTs array after 10 s of deposition. These particles contain Cu according to the EDX analysis reported in Fig. 8. For longer deposition times, the morphology changes significantly, as shown in Fig. 9, where the large amount of deposited material covers the pores' mouth. The presence of Cu_2O was confirmed by EDX elemental analysis (see Fig. 10).
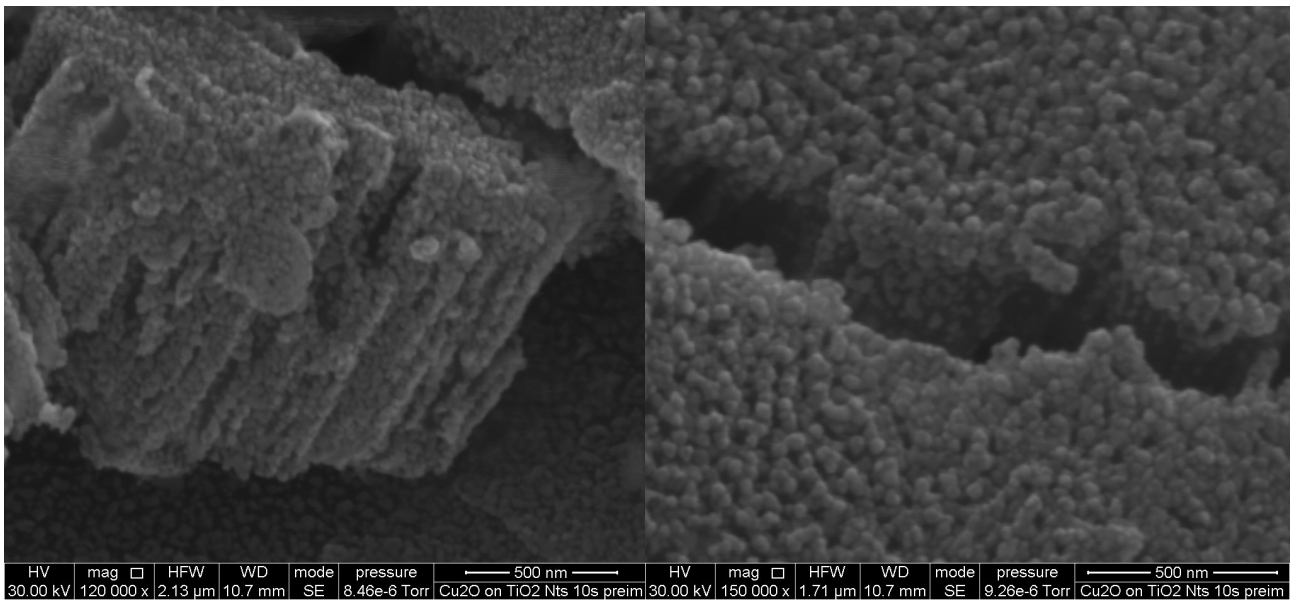
9

Figure 7 – Side views of TiO$_2$ NTs array, prepared in ethylene glycol (45 V for 10 minute) and annealed at 450°C for 20 minutes, after 10 s of electrodeposition.
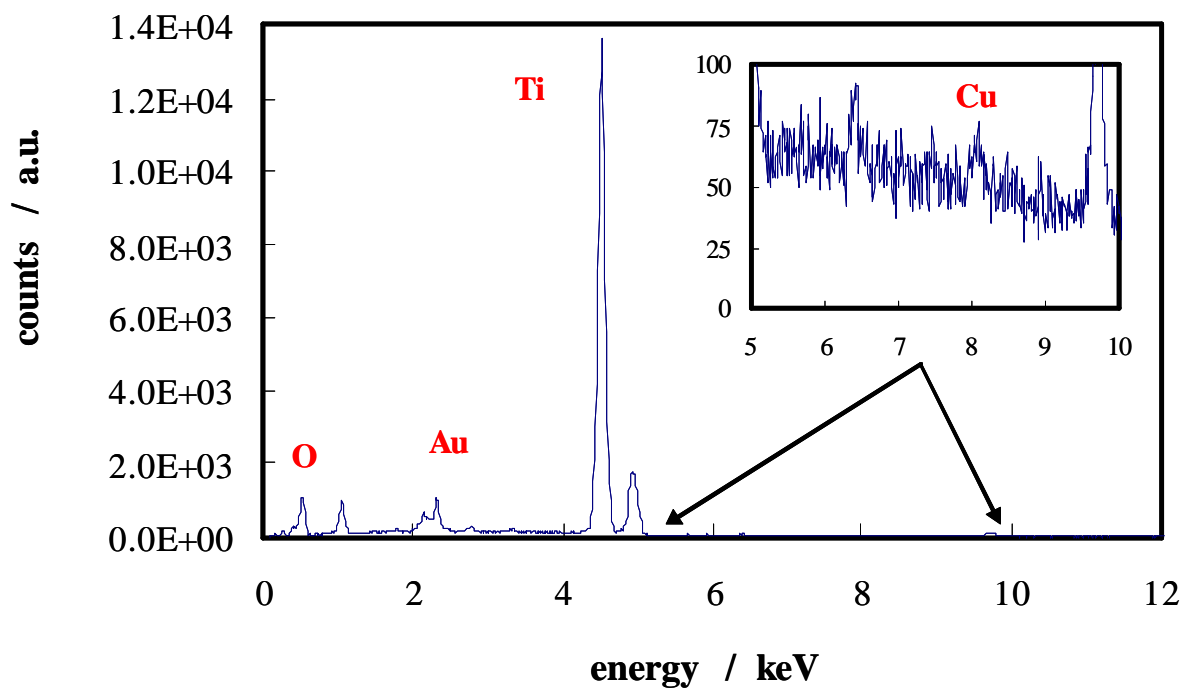

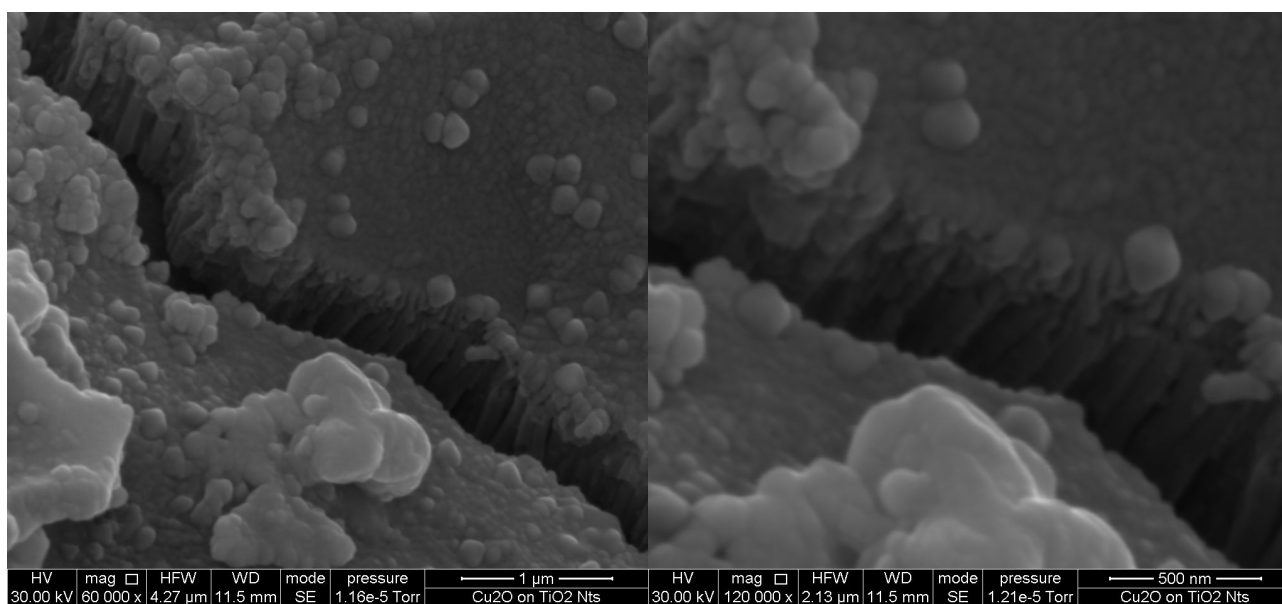**Figure 8** – EDX spectrum relating to the sample of Fig. 7.

Figure 9 –TiO₂ NTs array prepared in ethylene glycol (45 V for 10 minute) and annealed at 450°C for 20 minutes, after 5 minutes of electrodeposition.
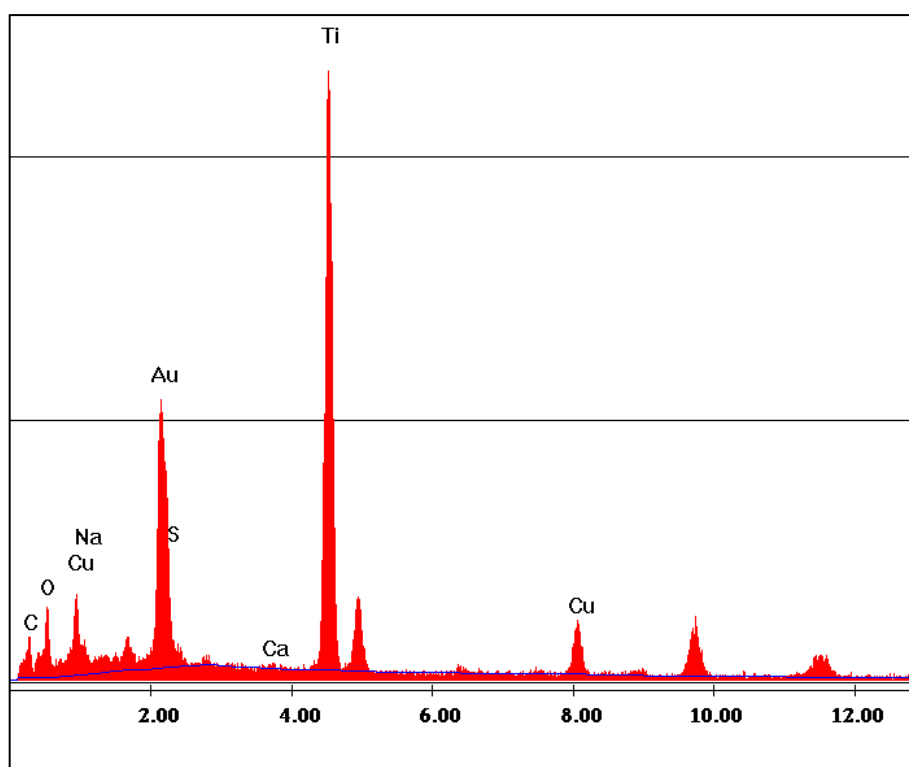

Figure 10 – EDX spectrum relating to the sample of Fig. 9.

The deposition of Cu_2O was confirmed by XRD diffraction patterns. In Fig. 11 we report the X-ray diffraction pattern relating to Ti/TiO_2 NTs electrode after 5 min of electrodeposition. Apart from the diffraction peaks attributed to anatase and to Ti substrate, a peak at $2\theta = 36.42°$ is present, which can be attributed to the <111> direction of cubic Cu_2O according to ICCD card 05-0667.
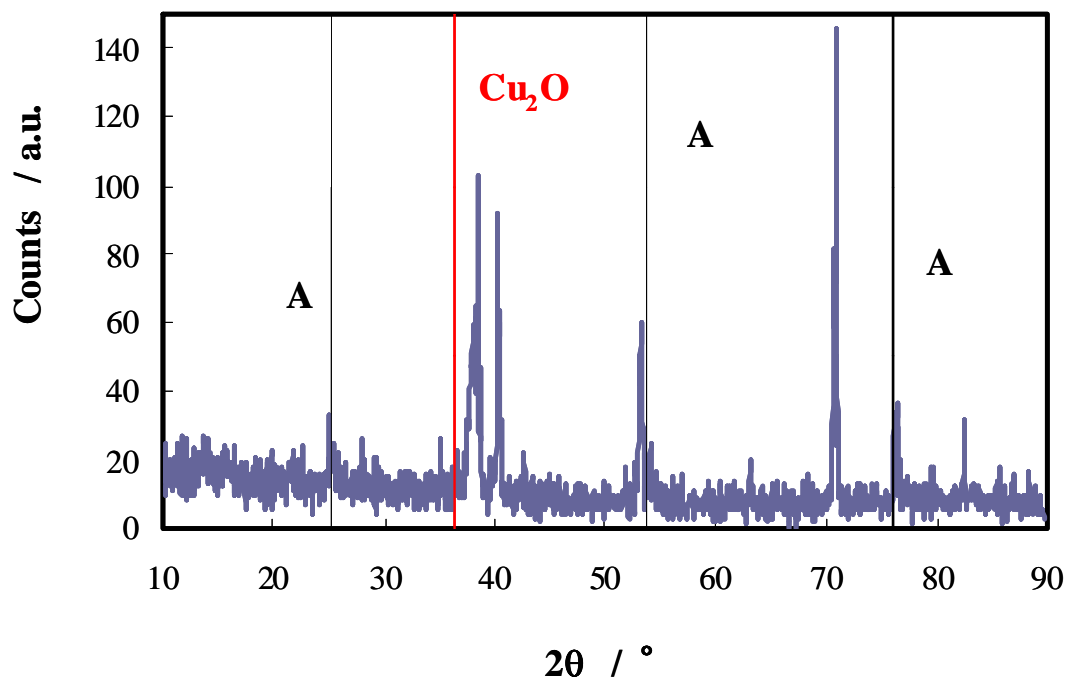

Figure 11 - XRD diffraction pattern relating to TiO_2 nanotubes after 5 min of electrodeposition. Peaks labelled as A are ascribed to anatase (ICCD card 21-1272), while those not labelled are ascribed to Ti: substrate (ICCD card 44-1294).

In order to evidence the effect of Cu_2O on the photoelectrochemical behaviour of TiO_2 NTs, we recorded photocurrent spectra at the open circuit potential ($\sim 0.05 \pm 0.05$ V) and at 0.15 V. No appreciable differences were evidenced for nanotubes after 10 s of deposition, while the presence of Cu_2O strongly influenced the photoelectrochemical behaviour of the TiO_2 NTs after 5 min of deposition. In Fig. 12 we compare the raw photocurrent spectra relating to TiO_2 nanotubes soon after annealing and after 5 min of electrodeposition, recorded by polarizing the electrodes at 0.15 V. The comparison shows that at low wavelength, a reduced photocurrent is measured as a consequence of the electrodeposition, while at high wavelength a significant increase in the measured photocurrent is revealed. The presence of Cu_2O shifted the absorption threshold toward lower energy so that it was possible to record under chopped light with a UV filter the photocurrent tail reported in Fig. 13.
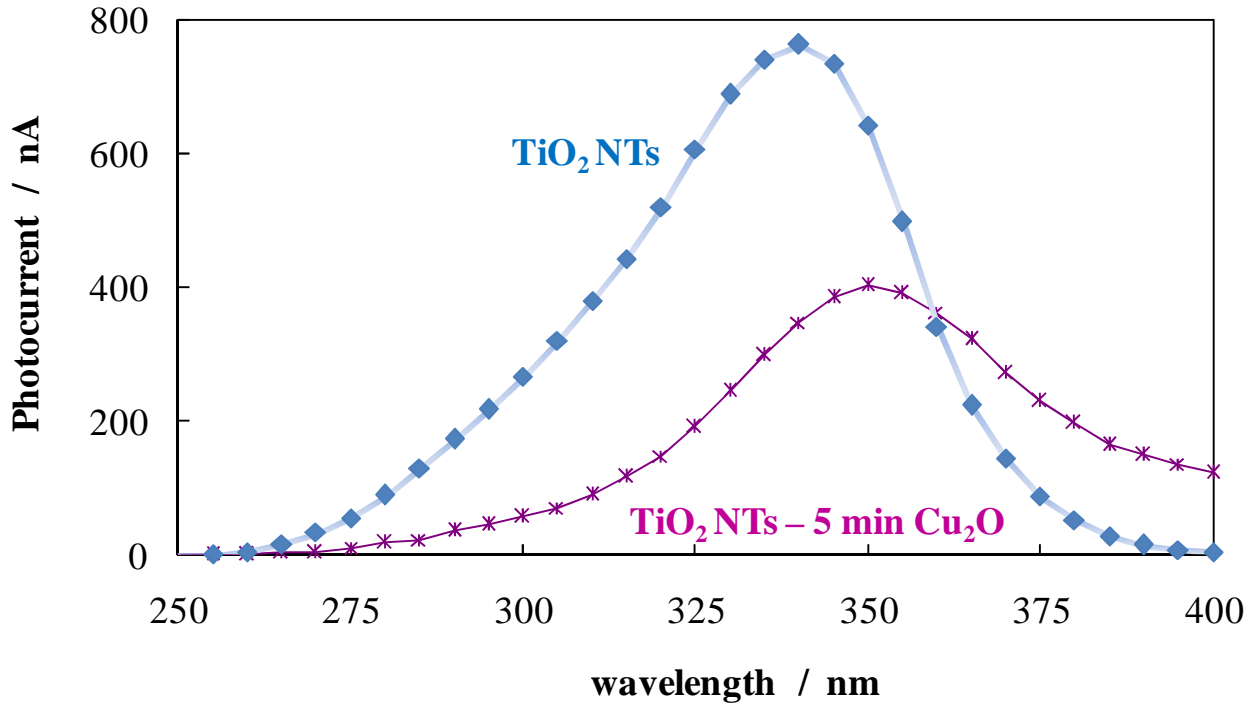
12

Figure 12 – Raw photocurrent spectra relating to TiO$_2$ nanotubes soon after annealing and after 5 min of electrodeposition.
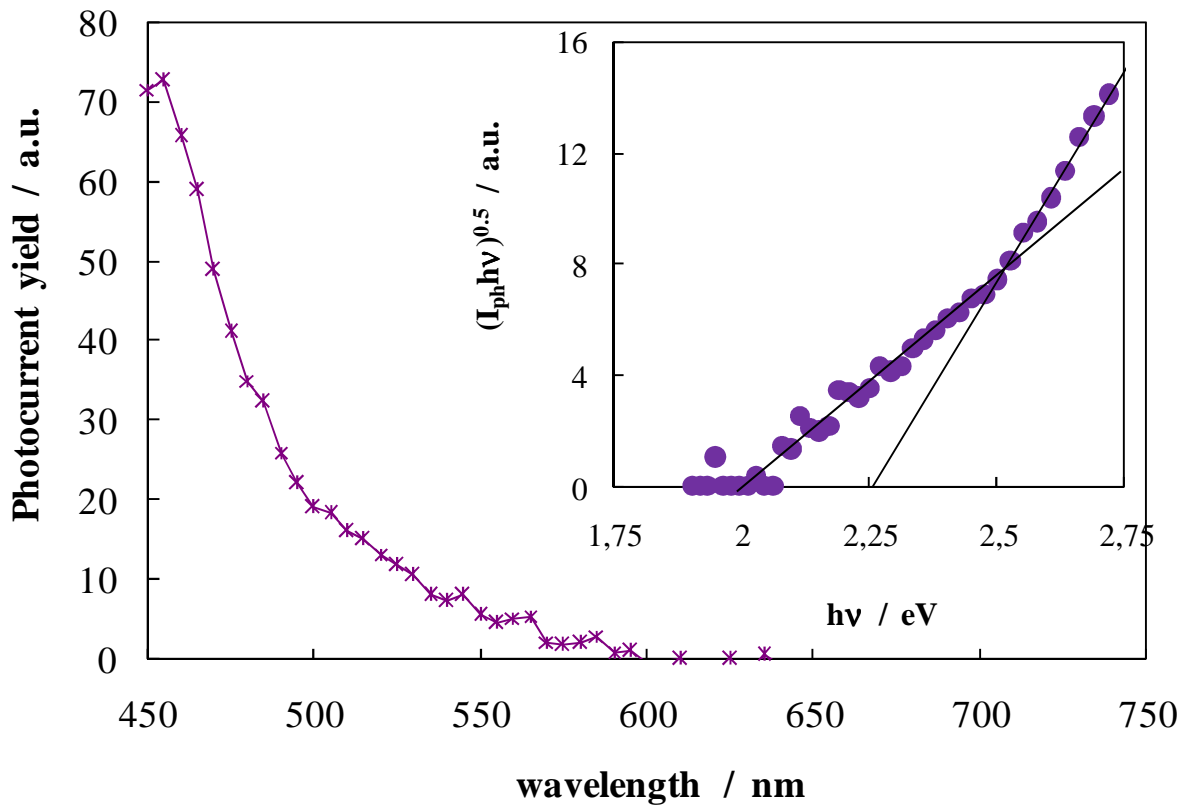

Figure 13 – Photocurrent spectrum relating to TiO$_2$ nanotubes soon after annealing and 5 min of electrodeposition. U$_E$ = 0.15 V.

Two linear regions are present in the $(I_{ph}h\nu)^{0.5}$ vs $h\nu$ plot, corresponding to optical transitions at 2.25 eV and 2.0 eV, the latter being very close to the band gap value of Cu_2O. It is noteworthy that direct optical transitions at 2.25 eV were also detected, as often observed with nano-crystalline Cu_2O.

In Fig. 14 we report the current vs time curves, recorded by polarizing the electrodes at constant potential under manually chopped irradiation at constant wavelength. The comparison of Fig. 3 and Fig. 14 shows that the presence of Cu_2O allows to measure higher photocurrent values especially at lower energy and that the absorption threshold of TiO_2 NTs/Cu_2O is significantly shifted toward lower energy, so that photocurrent can be measured even at $\lambda = 550$ nm. In Fig. 15 we report the I_{ph} values as a function of the irradiating wavelength, estimated from the current vs time curves under manually chopped light at 0.15 V. Each point for the TiO_2 NTs/Cu_2O junction is averaged at least for three runs. It is important to stress that he effect of cuprous oxide is significant at lower energy.
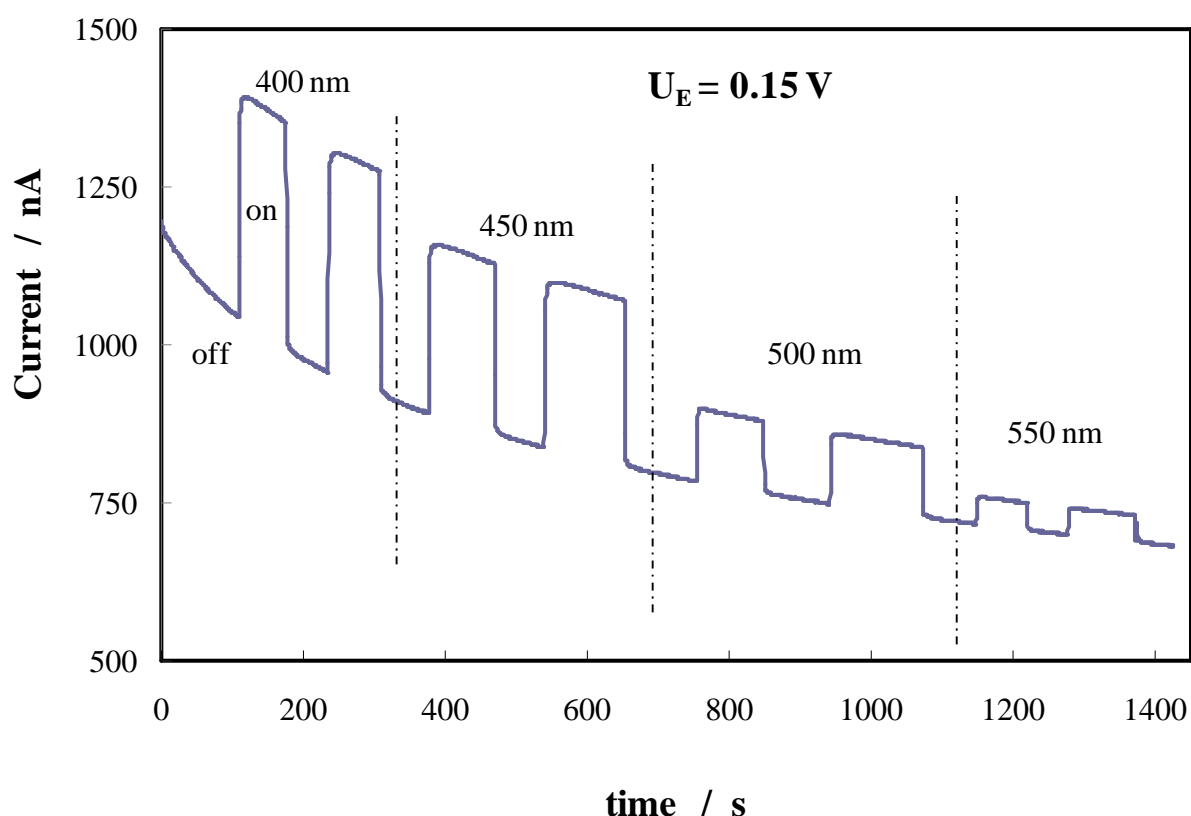

Figure 14 - Current vs time curves relating TiO_2 NTs after 5 min of Cu_2O electrodeposition under dark (off) or light (on) irradiation in 0.1 M Na_2SO_4.
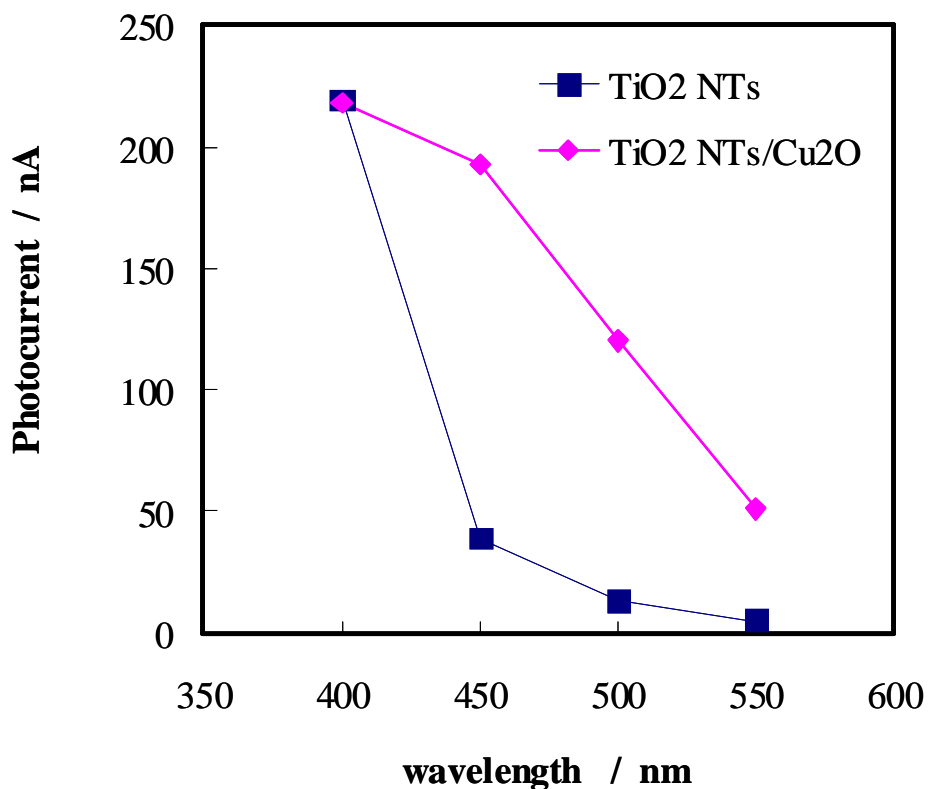
Figure 15 – Photocurrent intensity estimated from the I_{ph} vs time curves under manually chopped monochromatic light in 0.1 M Na_2SO_4 at 0.15 V.

It is interesting to mention that for deposition time longer than 5 minutes the photoelectrochemical behaviour of the prepared TiO_2-Cu_2O hetero-junction was found to be worse even with respect to not functionalized NTs, thus we expect that deposition time between 10 s and 5 minutes should be investigated. In Fig. 16 we report the current vs times curves recorded by polarizing the TiO_2 NTs after 30 s of electrodeposition (~ 18.2 mC cm^{-2}) under manually chopped irradiation at constant wavelength. By comparing the measured photocurrent values with those measured for longer deposition time, a sensitive improvement of the photoelectrochemical performance of the electrodes is evident. Finally, it is important to stress that these samples are photoactive even under 600 nm (i.e. 2.06 eV), thus confirming a strong shift in the light absorption threshold of this TiO_2-Cu_2O eterojunction with respect to not functionalized TiO_2 NTs.
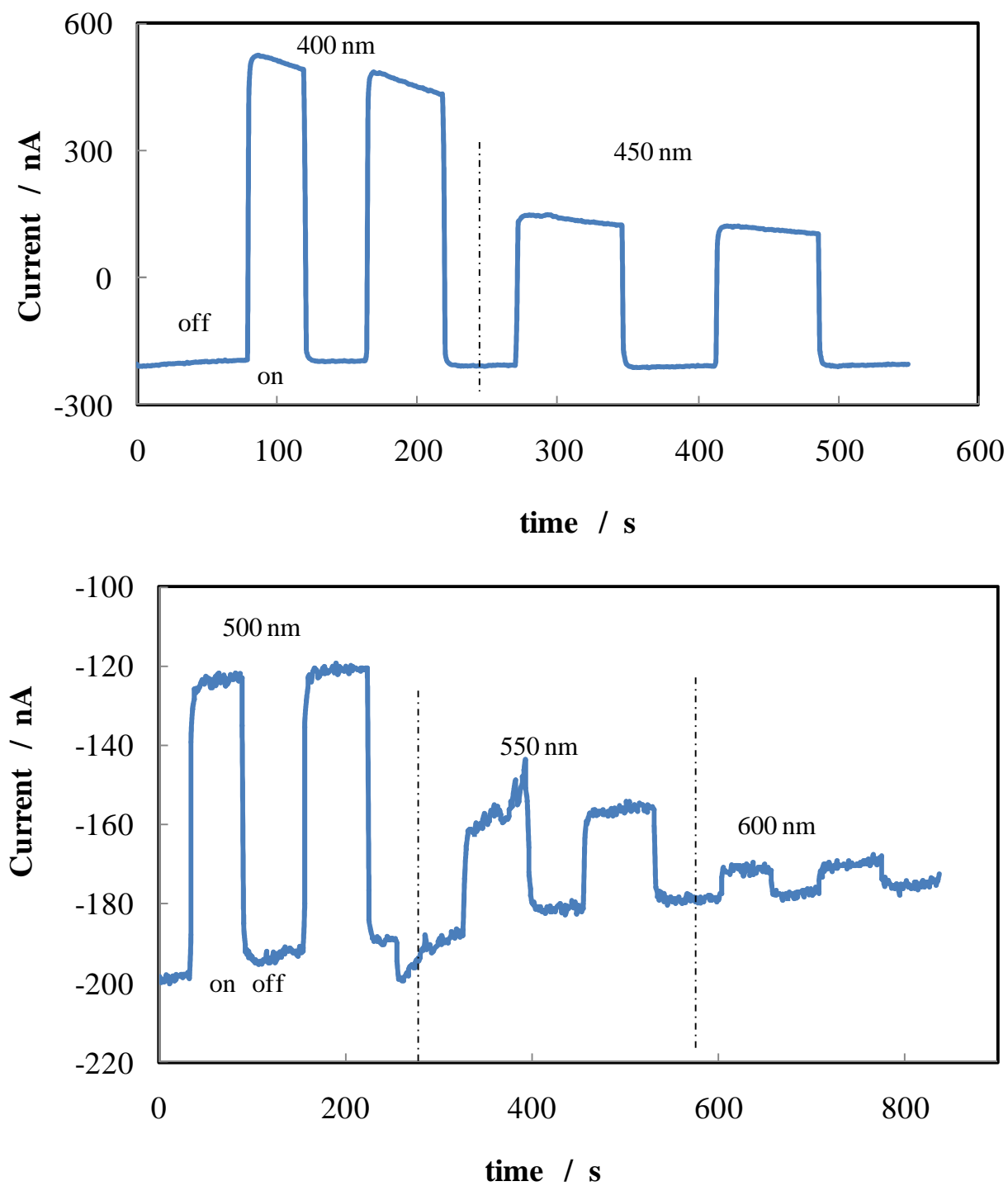
Figure 16 – Current vs time curves relating TiO$_2$ NTs after 30 s of Cu$_2$O electrodeposition under dark (off) or light (on) irradiation in 0.1 M Na$_2$SO$_4$. U$_E$ = U$_{OC}$ = 0.07 V.

Cu₂O cyclic voltammetric deposition

In Fig. 17 we report the current vs voltage curve, recorded by scanning the electrode potential at 20 mV s^{-1} from the open circuit voltage (~ 0 V) toward - 0.4 V (forward scan) and from - 0.4 to 0.1 V. The current increases monotonically by increasing the polarizing voltage in the cathodic direction. In spite of the oxygen reduction process, in this potential range reaction (1) is thermodynamically possible, thus we expect the Cu₂O deposition according to eq. (2). The morphology of the deposited layers is shown in Fig. 18, where we report the SEM micrographs relating to TiO₂ NTs after the deposition. Even if the overall charge circulated during the potential sweep is ~ 15.8 mC cm^{-2}, which is roughly 1/5 with respect to that circulated after 5 minutes of potentiostatic deposition (see Fig. 6), a continuous layer covers the pores' mouth, which contains copper according to the EDX analysis. Moreover, a small peak is present at 2θ = 36.42° in the XRD pattern, allowing for the identification of Cu₂O (see Fig. 19).
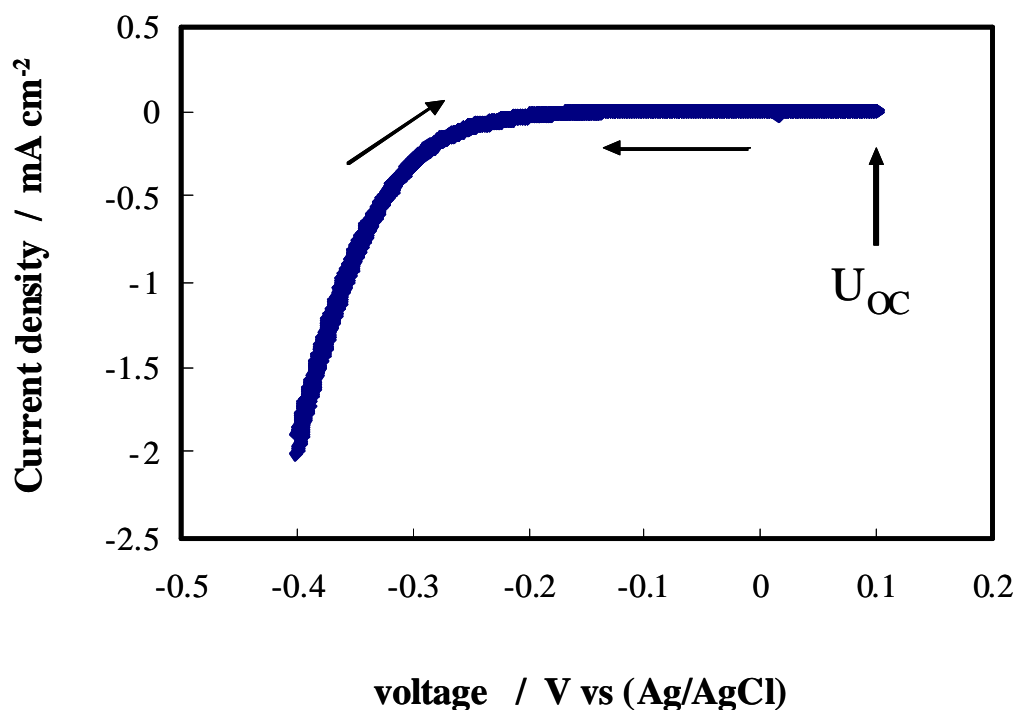

Figure 17 – Current density vs time curves recorded by scanning the potential of TiO₂ NTs at 20 mV s^{-1} in the electrodeposition solution (see experimental section).
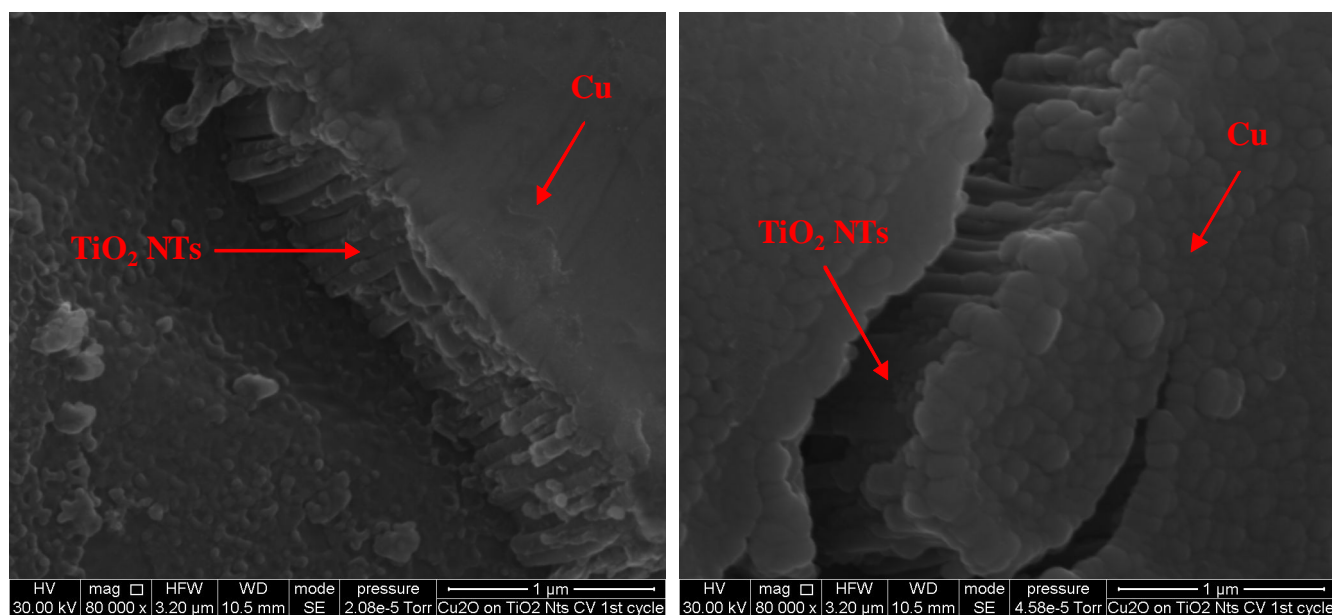
Figure 18 –TiO$_2$ NTs array prepared in ethylene glycol (45 V for 10 minute) and annealed at 450°C for 20 minutes, after the potential sweep in the electrodeposition solution reported in Fig. 17.
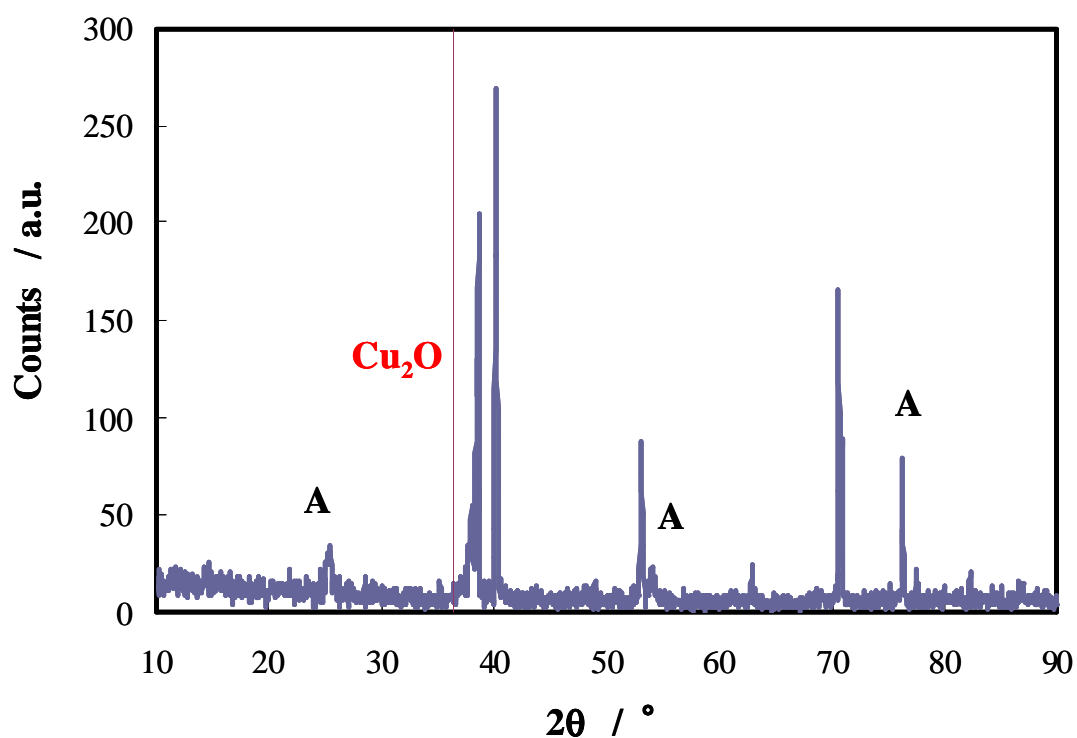

Figure 19 - XRD diffraction pattern relating to TiO$_2$ nanotubes after the potential sweep of Fig. 17. Peaks labelled as A are ascribed to anatase (ICCD card 21-1272), while those not labelled are ascribed to Ti substrate (ICCD card 44-1294).

In Fig. 20 we report the EIS spectrum relating to the TiO_2 NTs after the potential sweeps of Fig. 17. The dependence on frequency of both |Z| and phase angle of the measured impedance are very similar to that shown in Fig 4 for the TiO_2 NTs layer soon after annealing. Even the fitting parameters estimated according to the equivalent circuit of Fig. 4 are almost coincident with those estimated for Cu_2O free nanotubes. Thus, the presence of a cuprous oxide overlayer does not influence significantly the electrical behaviour of the electrode.
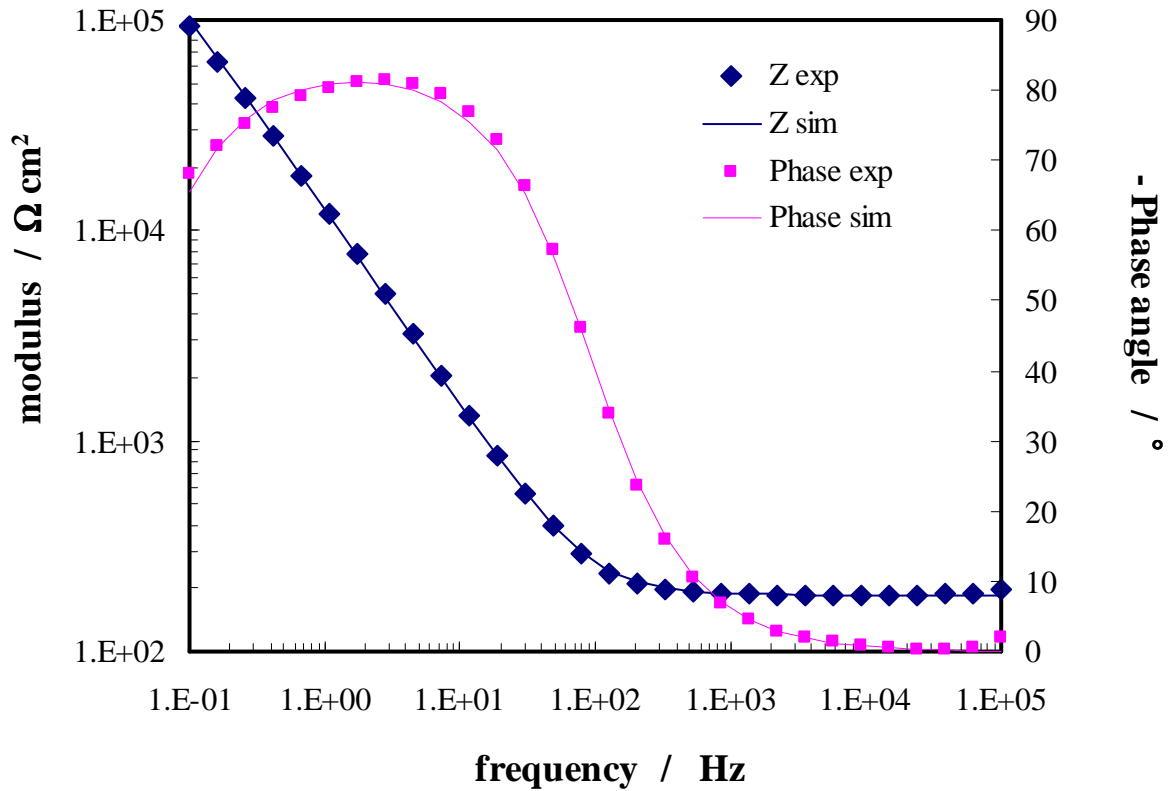

Figure 20 - Measured and simulated impedance and phase angles values relating to the TiO_2 NTs after thermal treatment, recorded by polarizing the electrode of Fig 16 at 0.15 V in 0.1 M Na_2SO_4.

Table 2 - Fitting parameters of Fig. 20.

R_{el} Ω cm^2	C_H μF cm^{-2}	R_{ox} Ω cm^2	Q_{ox} S cm^{-2}	n
186	31.5	$8 \cdot 10^4$	$2.3 \cdot 10^{-5}$	0.91

In Fig. 21 we report the current vs time curves recorded at constant potential (0.15 V) by irradiating the electrode with monochromatic light. The measured stationary I_{ph} are higher than those measured with not functionalized nanotubes but lower than that measured with TiO_2 NTs after 30 s of electrodeposition, in spite of very close values of charge density.
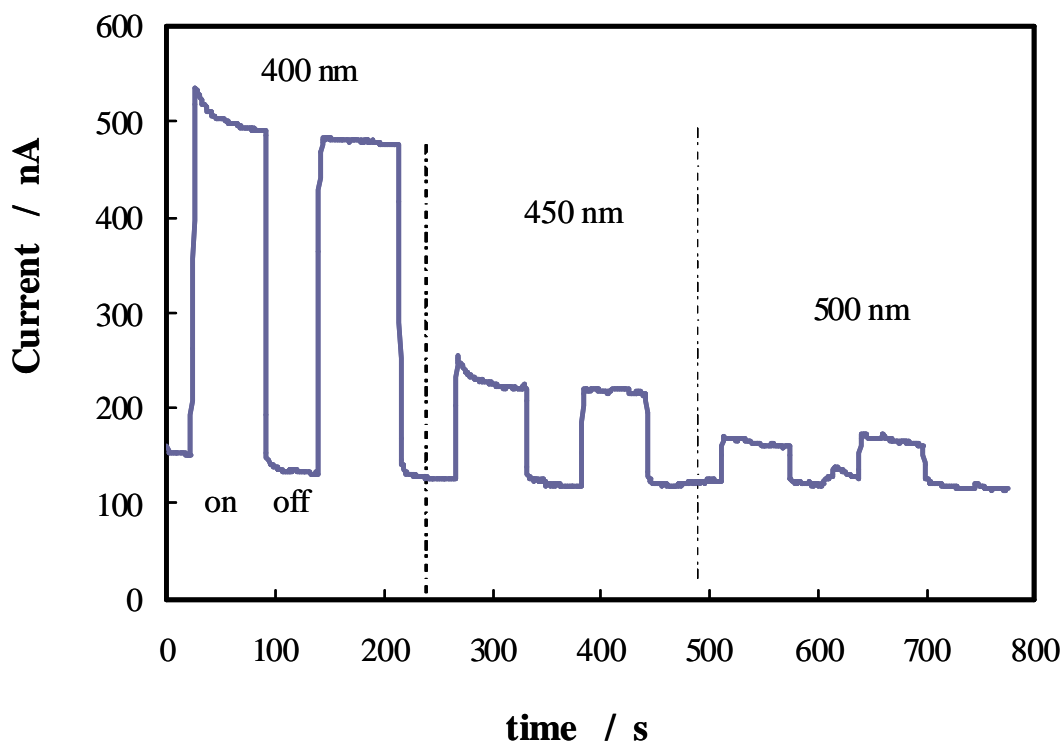

Figure 21 - Current vs time curves relating TiO_2 NTs after cyclic voltammetric electrodeposition (see Fig. 17) under dark (off) or light (on) irradiation in 0.1 M Na_2SO_4 at $U_E = 0.15$ V.

Conclusions

The Cu_2O electrodeposition process on TiO_2 NTs was studied in order to prepare TiO_2-Cu_2O hetero-junctions with a light absorption threshold lower than that of titanium oxide.

The electrodeposition was performed under potentiostatic regime ($U_E = -0.4$ V) for different time intervals. According to the morphology of the samples, even at the early stage of electrodeposition the whole surface of the TiO_2 nanotubes is covered by Cu_2O, which was identified by EDX and XRD analysis. However, the effect of cuprous oxide on the photoelectrochemical behaviour of the TiO_2 nanotubes is negligible for 10 s of electrodeposition (charge density ~2 mC cm^{-2}), while becomes sensitive after 5 minutes (charge density ~87 mC cm^{-2}). For these samples a significant red shift in the light-absorption edge was evidenced, due to the presence of Cu_2O.

20

The photoelectrochemical performance of the electrodes did not improve for longer deposition times (i.e. 10 minutes), while a significant improvement was obtained at intermediate deposition times (charge densities). According to the current vs times curves, recorded under manually chopped light, very promising results can be obtained with TiO_2 NTs layer after 30 s of electrodeposition (18.2 mC cm^{-2}). Finally, the experimental findings suggest that although we deposit on TiO_2 surface a comparable amount of Cu_2O during a potential sweep, the electrodes resulted less efficient than those prepared potentiostatically. These results suggest that the choice of the electrical variables during the deposition steps of the inorganic sensitizer, Cu_2O, can be a crucial step toward the improvement of the photoresponse of TiO_2 photoelectrodes.

References

1 - A. Fujishima, T. N. Rao, and D. A. Tryk, J. Photochem. Photobiol. C 1, 1   2000

2 - X. B. Chen and S. S. Mao, Chem. Rev. (Washington, D.C) 107, 2891 (2007).

3 - T. Berger, M. Sterrer, O. Diwald, D. Panayotov, T. L. Thompson, and J. T. Yates, Jr., J. Phys. Chem. B 109, 6061   2005.

4 - Q. P. Wu, D. Z. Li, L. Wu, J. Wang, X. Z. Fu, and X. X. Wang, J. Mater. Chem. 16, 1116   2006.

5 - J. Georgieva, S. Armyanov, E. Valova, I. Poulios, and S. Sotiropoulos, Electrochem. Commun. 9, 365, 2007.

6 - M. K. Lee and T. H. Shih, J. Electrochem. Soc. 154, P49   2007.

7 - V. F. Puntes, K. M. Krishnan, and A. P. Alivisatos, Science 291, 2115, 2001.

8 - R. Jin, Y. W. Cao, C. A. Mirkin, K. L. Kelly, G. C. Schatz, and J. G. Zheng, Science 294, 1901   2001.

9 - Y. Bessekhouad, D. Robert, and J. V. Weber, Catal. Today 101, 315, 2005.

10 - W. Siripala, A. Ivanovskaya, T. F. Jaramillo, S. Baeck, and E. W. McFerland,Sol. Energy Mater. Sol. Cells, 77, 229, 2003.

11 - N. Helaïli, Y. Bessekhouad, A. Bouguelia, and M. Trari, J. Hazard. Mater., 168, 484, 2009.

12 - F. Di Quarto, S. Piazza, M. Santamaria, C. Sunseri, Handbook of Thin Films, H. S. Nalwa, Vol. 2, p. 373, Academic Press, San Diego (2002)